Year: 2024

Quantifying neurodegeneration of the cervical cord and brain in degenerative cervical myelopathy : A multicentre study using quantitative magnetic resonance imaging

Freund, Patrick ; Boller, Viveka ; Emmenegger, Tim M ; Akbar, Muhammad ; Hupp, Markus ; Pfender, Nikolai ; Wheeler-Kingshott, Claudia Angela Michela Gandini ; Cohen-Adad, Julien ; Fehlings, Michael G ; Curt, Armin ; Seif, Maryam

ORIGINAL ARTICLE

Quantifying neurodegeneration of the cervical cord and brain in degenerative cervical myelopathy: A multicentre study using quantitative magnetic resonance imaging

Patrick Freund[1,2] | Viveka Boller[1] | Tim M. Emmenegger[1] | Muhammad Akbar[3] |
Markus Hupp[1] | Nikolai Pfender[1] | Claudia Angela Michela Gandini Wheeler-Kingshott[4,5,6] |
Julien Cohen-Adad[7,8] | Michael G. Fehlings[3] | Armin Curt[1] |
Maryam Seif[1,2]

[1]Spinal Cord Injury Centre, University Hospital Balgrist, University of Zurich, Zurich, Switzerland

[2]Department of Neurophysics, Max Planck Institute for Human Cognitive and Brain Sciences, Leipzig, Germany

[3]Spine Program Division of Neurosurgery, University of Toronto and Toronto Western Hospital, Toronto, Ontario, Canada

[4]NMR Research Unit, Queen Square MS Centre, University College London (UCL) Queen Square Institute of Neurology, Faculty of Brain Sciences, London, UK

[5]Department of Brain and Behavioral Sciences, University of Pavia, Pavia, Italy

[6]Digital Neuroscience Research Unit, IRCCS Mondino Foundation, Pavia, Italy

[7]NeuroPoly Lab, Institute of Biomedical Engineering, Polytechnique Montreal, Montreal, Quebec, Canada

[8]Functional Neuroimaging Unit, CRIUGM, University of Montreal, Montreal, Quebec, Canada

Correspondence
Maryam Seif, Spinal Cord Injury Centre, University Hospital Balgrist, University of Zurich, Forchstrasse 340, 8008 Zurich, Switzerland.
Email: maryam.seif@balgrist.ch

Funding information
Wings for Life, Grant/Award Number: WFL-CH-007/14 and WFL-CH-19/20; Schweizerischer Nationalfonds zur Förderung der Wissenschaftlichen Forschung, Grant/Award Number: 181362 by SNSF

Abstract

Background and purpose: Simultaneous assessment of neurodegeneration in both the cervical cord and brain across multiple centres can enhance the effectiveness of clinical trials. Thus, this study aims to simultaneously assess microstructural changes in the cervical cord and brain above the stenosis in degenerative cervical myelopathy (DCM) using quantitative magnetic resonance imaging (MRI) in a multicentre study.

Methods: We applied voxelwise analysis with a probabilistic brain/spinal cord template embedded in statistical parametric mappin (SPM-BSC) to process multi parametric mapping (MPM) including effective transverse relaxation rate (R2*), longitudinal relaxation rate (R1), and magnetization transfer (MT), which are indirectly sensitive to iron and myelin content. Regression analysis was conducted to establish associations between neurodegeneration and clinical impairment. Thirty-eight DCM patients (mean age $\pm$ SD$=58.45\pm11.47$ years) and 38 healthy controls (mean age $\pm$ SD$=41.18\pm12.75$ years) were recruited at University Hospital Balgrist, Switzerland and Toronto Western Hospital, Canada.

Results: Remote atrophy was observed in the cervical cord ($p=0.002$) and in the left thalamus (0.026) of the DCM group. R1 was decreased in the periaqueductal grey matter ($p=0.014$), thalamus ($p=0.001$), corpus callosum ($p=0.0001$), and cranial corticospinal tract ($p=0.03$). R2* was increased in the primary somatosensory cortices ($p=0.008$). Sensory impairments were associated with increased iron-sensitive R2* in the thalamus and periaqueductal grey matter in DCM.

Conclusions: Simultaneous assessment of the spinal cord and brain revealed DCM-induced demyelination, iron deposition, and atrophy. The extent of remote neurodegeneration was associated with sensory impairment, highlighting the intricate and expansive nature of microstructural neurodegeneration in DCM, reaching beyond the stenosis level.

KEYWORDS
brain, DCM, multicentre study, multiparametric mapping, spinal cord

INTRODUCTION

Degenerative cervical myelopathy (DCM) is the most common form of nontraumatic spinal cord injury in adults, with a rising incidence among the global ageing population [1, 2]. DCM-induced disability can differently manifest in individuals, spanning a spectrum from mild pain and minor hand numbness to severe cases of incomplete tetraplegia. These severe cases can result in long-lasting impairments of upper extremity function, gait difficulties, and bladder dysfunction [2]. DCM is characterized by chronic spinal cord compression, leading to neural tissue destruction at the site of compression, but also remote changes of the spinal cord [3, 4], and can even affect the brain [5, 6]. The current standard of care for moderate to severe DCM is surgical decompression. Nevertheless, in the case of mildly affected DCM patients, the ideal timing for surgical intervention remains uncertain. Additionally, it is worth noting that even after anatomically successful surgery, some DCM patients may still experience progressive disability [2].

Quantitative magnetic resonance imaging (qMRI) techniques have the potential to offer biomarkers that are sensitive to pathophysiological changes with clinical significance [7–11]. Consequently, these techniques hold promise for enhancing the prediction of recovery in patients with DCM [12] and helping with clinical decision-making [9]. The robustness and reproducibility of qMRI methods across multiple clinical sites are crucial prerequisites for the development of such biomarkers. Furthermore, there is a growing need to enhance statistical power to improve the efficiency of clinical trials [13–16]. We here use an established qMRI protocol sensitive to microstructural changes in the brain and cervical cord that has already been applied and validated in a multicentre study in healthy subjects in the scope of a European multicentre/multivendor clinical trial [13, 16]. These studies showed high repeatability and reproducibility of multiparametric mapping (MPM) in the brain and cervical cord across different vendors and sites.

To simultaneously track changes in the brain and cervical cord, we further make use of a probabilistic brain–spinal cord template (SPM-BSC) [17]. This approach has been successfully applied to traumatic spinal cord injury patients [18] and patients with multiple sclerosis [19]. We aim to simultaneously map the regional distribution of neurodegeneration in the brain and cervical cord in patients with mild–moderate DCM by means of qMRI. We further aim to assess the effects of the severity of intramedullary injury (i.e., radiologically established cervical myelopathy) on remote microstructural changes and clinical impairments.

MATERIALS AND METHODS

This prospective study was in accordance with the Declaration of Helsinki, approved by the local ethics committee (EK-2010-0271, 16-5149-AE) and registered (www.clinicaltrials.gov; NCT 02170155) in Zurich and Toronto. Informed written consent was obtained from each participant before study enrolment. Study data were collected and managed using REDCap electronic data capture tools hosted at Balgrist University Hospital, Zurich, Switzerland.

Study population

Thirty-eight mild–moderate DCM patients (19 DCM patients with radiologically established cervical myelopathy, i.e., T2-weighted hyperintensity) were recruited between 2017 and 2019, of whom 24 were recruited at University Hospital Balgrist, Zurich, Switzerland from the spine surgery outpatient clinic and 14 were recruited at Toronto Western Hospital, Canada with mild ($n = 30$, with modified Japanese Orthopaedic Association [mJOA] score ≥ 15) to moderate injury ($n = 8$ with 12 ≤ mJOA ≤ 14; mean age ± SD = 58.45 ± 11.47 years, eight females). The healthy controls were significantly younger than the DCM group ($p < 0.001$). Moreover, 38 healthy participants (mean age ± SD = 41.18 ± 12.75 years, seven females, of whom 24 subjects were from University Hospital Balgrist and 14 were from Toronto Western Hospital) were recruited. Inclusion criteria for DCM patients were degenerative cervical spinal cord compression with focal myelopathy on MRI and/or clinical signs and symptoms of cervical myelopathy (i.e., clumsy hands, segmental sensory deficits, pain, gait disturbances, and bladder dysfunction) [20]. The exclusion criteria for all participants were previous spine operations, pregnancy, head or brain lesions, pre-existing neurological and medical disorders leading to functional impairments, mental disorder, contraindications to MRI, and age < 18 or > 70 years. For patients with suspicion of any other neurological disease (e.g., radiculopathy at the lower limbs, polyneuropathy, central nervous system disorders), further examinations (e.g., cranial MRI, electrophysiologic examinations) were conducted prior to study inclusion. Next, the patient cohort was subclassified into two subgroups; DCM patients were assigned based on the presence or absence of radiological evidence of myelopathy in the cervical cord assessed by the occurrence of a hyperintense signal on the T2-weighted MRI of the lesion site.

Clinical assessments

All patients underwent a clinical examination specific to DCM including the mJOA score and the Nurick scale. The mJOA score is a validated disease-specific outcome measurement quantifying clinical impairment in the upper and lower limbs as well as sphincter function on an 18-point scale as follows [21]: a score of 18 reflects no impairment, whereas lower scores indicate a progressively greater degree of disability and functional impairment. In addition, the Nurick classification [22] was conducted to grade patients into six different categories, from 0 to 5, where a grade of 0 indicates no evidence of spinal cord involvement to the patient's symptoms and a grade of 5 indicates a patient chairbound or bedridden. Moreover, the upper limb function of patients was assessed by applying the sensory subset of Graded Redefined Assessment of Strength,

Sensibility and Prehension (GRASSP) as an ancillary outcome measure dedicated to the assessment of DCM patients [23]. Additionally, the International Standards for Neurological Classification of Spinal Cord Injury protocol [24] was performed, which discerns detailed assessments of the upper and lower extremity motor function, as well as light-touch and pinprick sensation across C2 to T1.

MRI acquisition

MRI measurements were performed in a head-first supine position on a Siemens 3T MRI (Skyra) Scanner (Siemens Healthineers, Erlangen, Germany) at the University Hospital Balgrist Zurich and Toronto Western Hospital equipped with a 20-channel radiofrequency (RF) receiver head and neck coil. For structural evaluation purposes, two-dimensional (2D) sagittal T2-weighted MRI was performed at the lesion level covering the entire cervical cord with the following parameters: repetition time (TR)=3500ms, echo time (TE)=84ms, flip angle=160°, field of view=$220 \times 220 \, mm^2$, in-plane resolution=$0.34 \times 0.34 \, mm^2$ with interpolation and slice thickness of 2.5mm, and readout bandwidth=260Hz/pixel, demanding a total scan time of 1.37min. Additionally, at the maximum compression level, axial T2-weighted scans were performed with TR=5510ms, TE=96ms, flip angle=150°, field of view=$160 \times 160 \, mm^2$, in-plane resolution=$0.6 \times 0.6 \, mm^2$, and readout bandwidth=283Hz/pixel, resulting in a total scan time of 1.57min.

To quantify microstructural indices, the MPM protocol [13, 16, 25, 26] was applied covering both brain and cervical cord down to the C4 level with field of view of $224 \times 256 \, mm^2$. Three 3D fast low-angle shot gradient echo (FLASH) sequences with different parameters were performed to generate the different MRI contrast. The MPM protocol included acquisition of magnetization transfer (MT)-weighted, proton density (PD)-weighted, and T1-weighted MRI with isotropic resolution of $1.1 \times 1.1 \, mm^2$. TR=25ms and flip angle=23° were chosen for T1-weighted MRI, TR=25ms and flip angle=4° were chosen for PD-weighted MRI, and TR=37ms and flip angle=9° were chosen for MT-weighted MRI. Subsequent reconstruction was performed with the GRAPPA (generalized autocalibration partially parallel acquisition) algorithm in the anterior–posterior phase-encoding direction and a partial Fourier acquisition with a 6/8 sampling factor in the partition direction left–right. We used parallel imaging with an acceleration factor of 2 in both phase-encoding directions. Echoes were acquired at six equidistant echo times from 2.46 to 14.76ms for all FLASH sequences, with an additional two echoes at 17.22 and 19.68ms for the PD-weighted and T1-weighted sequences. Total acquisition time was 23 min.

MRI processing

Lesion segmentation

The sagittal and axial T2-weighted magnetic resonance images of the lesions were used to determine the exact level(s) of spinal canal stenosis and intramedullary signal hyperintensity as a sign of myelopathy (radiological evidence of cervical myelopathy) along the cervical spinal cord. To show the distribution frequency of lesions in DCM patients, hyperintense voxels were manually segmented on axial slices using FSL-eyes from FMRIB software library v6.0. Next, the total spinal cord area was segmented and normalized to the T2-weighted PAM50 spinal cord template [27] in Spinal Cord Toolbox software (v3.2.2) [28] by applying slicewise nonlinear registration. A lesion frequency map was created to illustrate the distribution of lesions over vertebral levels and in the axial plane. In the lesion map, voxel intensity represents the frequency of a lesion (%) occurring in the corresponding voxel.

Simultaneous voxelwise quantification of brain and cervical cord microstructure

The voxel-based morphometry and MPM analysis in SPM-12 (v7219, MATLAB 2019b) were extended to include cervical spinal cord by incorporating a probabilistic atlas of the brain and neck (Figure 1) [17, 18]. In the first step, the acquired MRI data were reoriented in SPM-12. To assess the volumetric changes, the brain and spinal cord template was applied on the MT-weighted images of individuals to segment the MT map into several tissue classes such as grey matter (GM) and white matter (WM) in the brain. To assess morphological changes in the spinal cord, the native-space GM and WM tissue maps were combined to form a neural tissue (NT) class due to low contrast level in GM and WM at the cervical level [18]. A group-specific spinal cord mask was computed by thresholding the average of the NT maps of all subjects to include voxels with probability of >50% and further restricting this mask to the spinal cord at levels C1–C3 (visually defined). Next, the GM, WM, and NT maps were spatially normalized to MNI space with Dartel [29] and modulated by the Jacobian determinants of the deformations [30]. Finally, an isotropic Gaussian kernel of 6mm full width at half maximum (FWHM) was applied to the modulated tissue maps. The total intracranial volume was computed from the sum of the GM, WM, and cerebrospinal fluid (CSF) volumes [31]. The voxel-based microstructural assessment was based on the MT, longitudinal relaxation rate (R1), and effective transverse relaxation rate (R2*) quantitative maps derived from MPM images using the in vivo hMRI (histology MRI) toolbox [32]. Inhomogeneity of the RF transmit field was corrected using UNICORT [33, 34]. All tissue maps were transformed to MNI space using the Dartel algorithm [29]. MPMs were warped to the MNI space using participant-specific warping fields generated from the Dartel algorithm and finally smoothed using an isotropic Gaussian kernel filter with 6mm (in the GM) and with 4mm (in the WM) FWHM in the brain. Smoothing the spinal cord images can results into undesired partial volume effects with CSF; therefore, we considered no smoothing for the cord prior to statistical analysis [18]. For statistical analysis, we excluded all voxels with a GM probability <0.2 and WM probability <0.6 to minimize contribution from partial volume effects near GM/WM borders. Quality assessments were conducted after each processing step using visual inspections by imaging experts. The spinal cord MPM parameters were additionally extracted within SPM based on the spinal cord mask to investigate the microstructural changes.
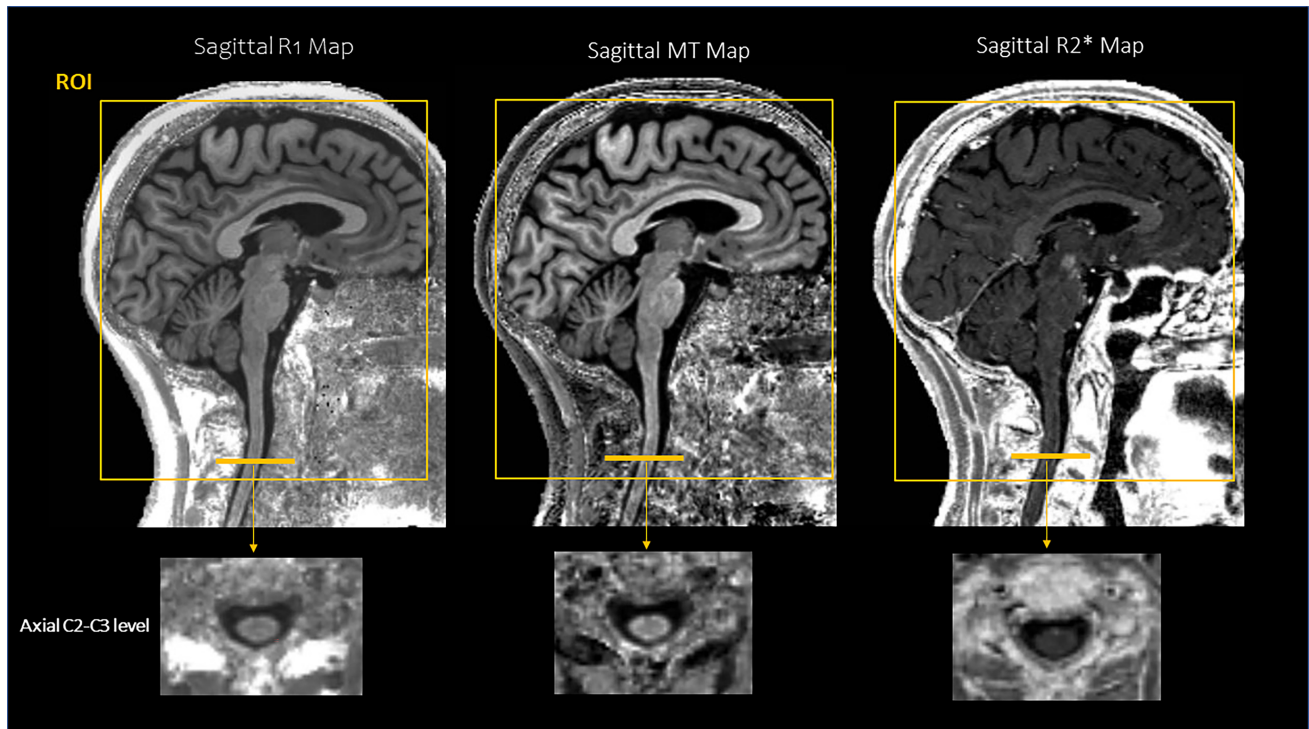
FIGURE 1 Representing multiparametric maps sagittal (longitudinal relaxation rate [R1], magnetization transfer [MT], and effective transverse relaxation rate [R2*]) from a degenerative cervical myelopathy patient's example. The figure shows the maps of both the brain and spinal cord, generated using the hMRI toolbox before applying normalization and segmentation. ROI, region of interest.

Statistical analysis

Statistical analyses describing the study population and correlations were conducted using the software R Studio (RStudio PBS, v1.4.1717). Voxelwise comparisons and multiple regression analyses were performed in SPM-12 (v7219). Descriptive analysis of demographic information was conducted by applying parametric and nonparametric statistics. The distribution of the data was assessed with the Shapiro–Wilk test. Subsequently, a *t*-test, in the case of normally distributed data, or a Wilcoxon rank-sum test (Mann–Whitney *U*-test), in the case of a nonnormal distribution, was performed to test for differences in the mean values between DCM patients and healthy controls. The same statistical tests were used to compare clinical outcome measures between the two DCM subgroups (i.e., with and without radiological evidence of myelopathy). Examining differences in distribution of sex among the groups, a Fisher exact test was applied. All results with statistical power of $p < 0.05$ were considered significant.

To assess microstructural changes in DCM patients compared with healthy controls, a voxelwise multiple regression analysis (within the factorial design in SPM-12) in the framework of a general linear model was applied. Furthermore, a voxelwise regression analysis was conducted to correlate the volumetric and microstructural changes to the clinical readouts in DCM patients. Age, sex, and clinical site were included as covariates of no interest. Total intracranial volume was additionally considered as a covariate in the voxel-based morphometry analysis for determining the tissue atrophy. To correct for multiple comparisons, only clusters surpassing a familywise error threshold of $p < 0.05$ were considered significant. A region of interest approach was applied to investigate changes of the sensorimotor system within the brain in the voxelwise analysis as follows: primary somatosensory cortex and the primary motor cortex; the cerebellum and cranial corticospinal tract; and the corpus callosum, thalami, and brainstem (excluding corticospinal tract region from the mask) [35, 36].

RESULTS

Demographic, clinical, and radiological characteristics

Of the 38 DCM patients (mean age $\pm$ SD $= 58.45 \pm 11.47$ years, eight females) included in the analysis, 30 showed a mild ($15 \leq$ mJOA ≤ 18) and eight a moderate ($12 \leq$ mJOA ≤ 14) degree of impairment. Twenty-two DCM patients had a multisegmental stenosis, and 16 patients were diagnosed with monostenosis. Nineteen (50%) DCM patients showed radiological signs of myelopathy, and 12 of those patients had multiple sites of stenosis (Table 1). Radiological evidence of myelopathy was frequently observed between the levels of C4 and C6, with a probability of up to 50% (Figure 2). There was no significant difference in clinical status between those patients with radiological evidence of myelopathy and those without myelopathy (Table 1).

TABLE 1 Study population demographics of degenerative cervical myelopathy patients.

ID	Sex	Age, years	Myelopathy	Maximum compression level	mJOA	Nurick	UEMS	Total cervical light touch (C2–T1)	Total cervical pin prick (C2–T1)
1	Female	51	No	C5/C6[a]	17	1	50	28	27
2	Male	77	No	C6/C7	16	1	50	32	28
3	Female	67	Yes	C5/C6[a]	16	1	48	32	30
4	Male	53	No	C5/C6[a]	15	1	50	31	29
5	Male	39	No	C5/C6[a]	17	1	50	24	24
6	Male	58	No	C6/C7[a]	17	0	50	31	32
7	Female	47	No	C5/C6	18	0	47	32	32
8	Female	50	Yes	C5/C6[a]	17	1	45	29	31
9	Male	56	Yes	C5/C6[a]	17	2	50	16	19
10	Male	45	No	C5/C6[a]	17	1	49	32	31
11	Female	34	Yes	C5/C6	14	2	50	26	27
12	Male	55	No	C5/C6	17	1	50	17	15
13	Male	62	Yes	C3/C4[a]	18	1	50	22	17
14	Male	56	No	C5/C6	16	1	50	28	28
15	Male	57	No	C6/C7[a]	16	1	18	32	30
16	Male	66	No	C5/C6	15	2	50	32	32
17	Female	51	No	C5/C6	12	1	50	24	24
18	Male	55	Yes	C5/C6[a]	16	1	50	32	30
19	Female	36	Yes	C5/C6	18	0	50	32	32
20	Male	59	Yes	C5/C6[a]	14	2	50	29	29
21	Male	62	Yes	C4/C5	18	0	50	32	32
22	Female	69	No	C4/C5[a]	18	0	49	32	32
23	Male	71	Yes	C5/C6	18	0	NA	32	32
24	Male	42	No	C5/C6	13	1	NA	25	26
25	Female	70	No	C5/C6	14	2	NA	NA	NA
26	Male	41	No	C5/C6[a]	15	2	NA	NA	NA
27	Female	80	No	C5/C6[a]	17	1	NA	NA	NA
28	Male	75	Yes	C3/C4[a]	17	1	NA	NA	NA
29	Female	71	Yes	C5/C6[a]	16	3	NA	NA	NA
30	Female	63	Yes	C3/C4	13	1	NA	NA	NA
31	Male	62	Yes	C3/C4[a]	17	3	NA	NA	NA
32	Female	46	Yes	C4/C5[a]	17	1	NA	NA	NA
33	Male	63	Yes	C6/C7	17	0	NA	NA	NA
34	Male	69	No	C5/C6	16	3	NA	NA	NA
35	Female	66	Yes	C5/C6[a]	14	3	NA	NA	NA
36	Male	70	Yes	C3/C4	16	2	NA	NA	NA
37	Female	60	No	C5/C6[a]	13	3	NA	NA	NA
38	Male	67	Yes	C2/C3[a]	18	0	NA	NA	NA

Note: Upper extremity cervical light touch maximum = 32 points; upper extremity cervical pinprick maximum = 32 points.

Abbreviations: mJOA, modified Japanese Orthopaedic Association (maximum = 18 points); NA, not available; UEMS, Upper Extremity Motor Score (maximum = 50 points).

[a]Multisegmental stenosis of the cervical spine.

Volumetric and microstructural changes in the cervical cord

Atrophy was evident in the cervical cord of DCM patients compared to healthy controls (Figure 3; z-score = 4.59, x = 2, y = −50, z = −72,

$p = 0.002$; Table 2). This atrophy was more pronounced in patients with radiological evidence of myelopathy than those patient without radiological evidence of myelopathy (Table 3). Patients without myelopathy had an increased iron-sensitive R2* in the cervical cord (z-score = 3.59, x = −2, y = −50, z = −98, $p = 0.024$; Table 3).
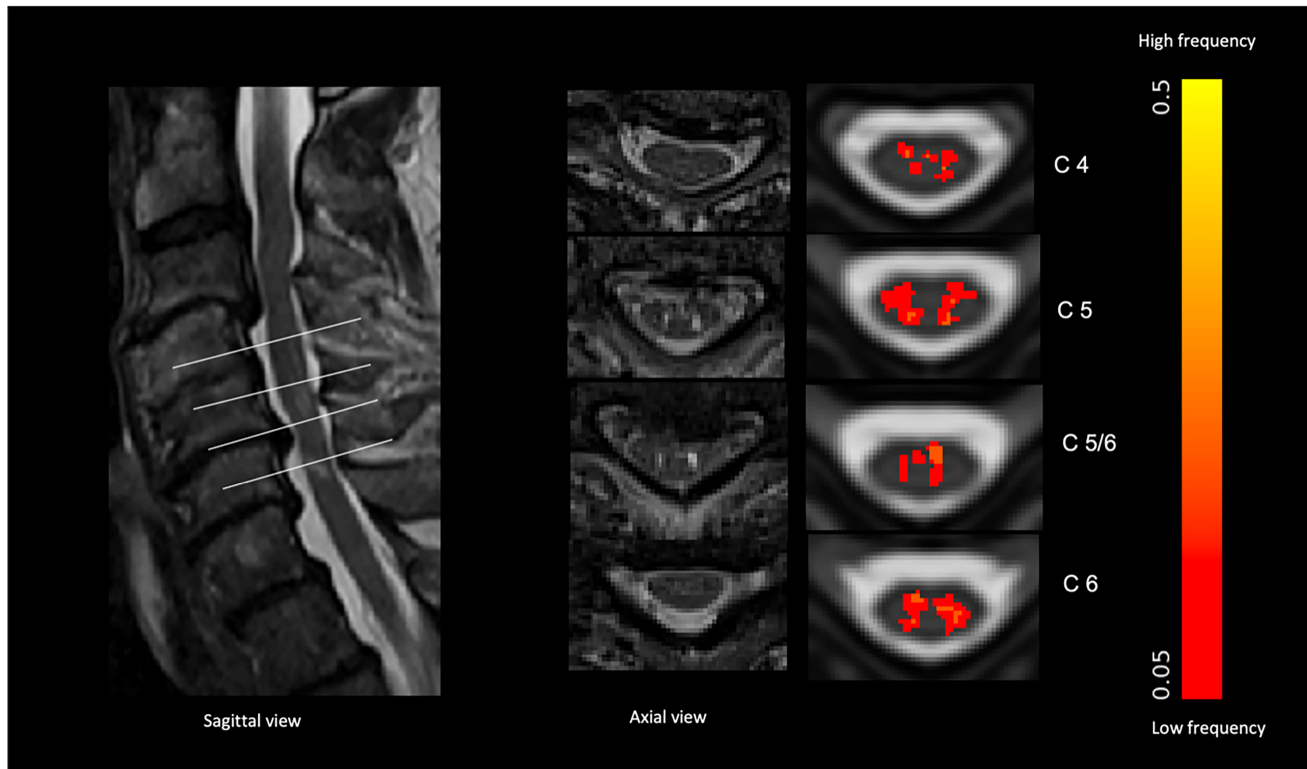
FIGURE 2 Frequency map represents the probability of each voxel showing a hyperintense signal. Red corresponds to a lower probability, whereas yellow indicates that in 50% of the included patients this particular voxel contributed to the hyperintense region.

Volumetric and microstructural changes in brain

In the brain, when comparing total DCM patients with healthy controls, atrophy was detected in the left thalamus (z-score = 4.07, x = −18, y = −23, z = 12, p = 0.026), whereas R1 was decreased in both thalami (z-score = 4.19, x = −15, y = −33, z = 8, p = 0.001), in the periaqueductal GM (PAG; z-score = 3.91, x = −11, y = −24, z = −17, p = 0.014), in the corpus callosum (z-score = 4.48, x = 3, y = −39, z = 20, p = 0.0001), and in the cranial corticospinal tracts (z-score = 4.06, x = −21, y = −29. z = 14, p = 0.03). Moreover, R2* increased in the left primary somatosensory cortex (z-score = 4.37, x = −44, y = −32, z = 51, p = 0.008; Table 2). However, the difference between MT in DCM and healthy controls did not appear statistically significant.

Association between severity of intramedullary damage, remote degeneration, and clinical outcomes

Regression analysis revealed that patients with established cervical radiological evidence of myelopathy were those with more remote atrophy in the left thalamus (z-score = 4.08, x = −17, y = −21, z = 15, p = 0.012). In parallel, R1 of those patients with radiological evidence of myelopathy decreased in both thalami (z-score = 3.97, x = −20, y = −27, z = 8, p = 0.001), in the left PAG (z-score = 3.85, x = −11, y = −24, z = −17, p = 0.032), in the corpus callosum (z-score = 4.29, x = 3, y = −39, z = 20, p = 0.001), and in the left corticospinal tract (z-score = 4.05, x = −21, y = −27, z = 15, p = 0.009).

Lower sensibility scores measured with the GRASSP test were associated with increased R2* in the PAG in DCM patients (z-score = 3.85, x = 2, y = −32, z = −6, p = 0.03, n = 33; Figure 4a). In addition, more impairment in the right sensibility scores was associated with increased R2* in the left thalamus (z-score = 3.41, x = −12, y = −24, z = 9, p = 0.047, n = 33; Figure 4b).

DISCUSSION

This multicentre study reveals simultaneously remote atrophy and microstructural neurodegeneration in the cervical cord and brain in mildly impaired DCM patients. The magnitude of these remote degenerative changes was associated with sensory impairments in DCM.

Assessment of cervical myelopathy

Clinical T2-weighted MRI of the lesion site showed hyperintensity, a characteristic observed in 50% of DCM patients (n = 19), indicating radiological evidence of myelopathy. The lesion frequency map discloses that intramedullary signal changes are observed with the highest probability from levels C4–C6, which are the segments with normally the maximum compression. This result was is in line with a previous report that included the patients recruited in Zurich [4]. The central GM was more involved in the development
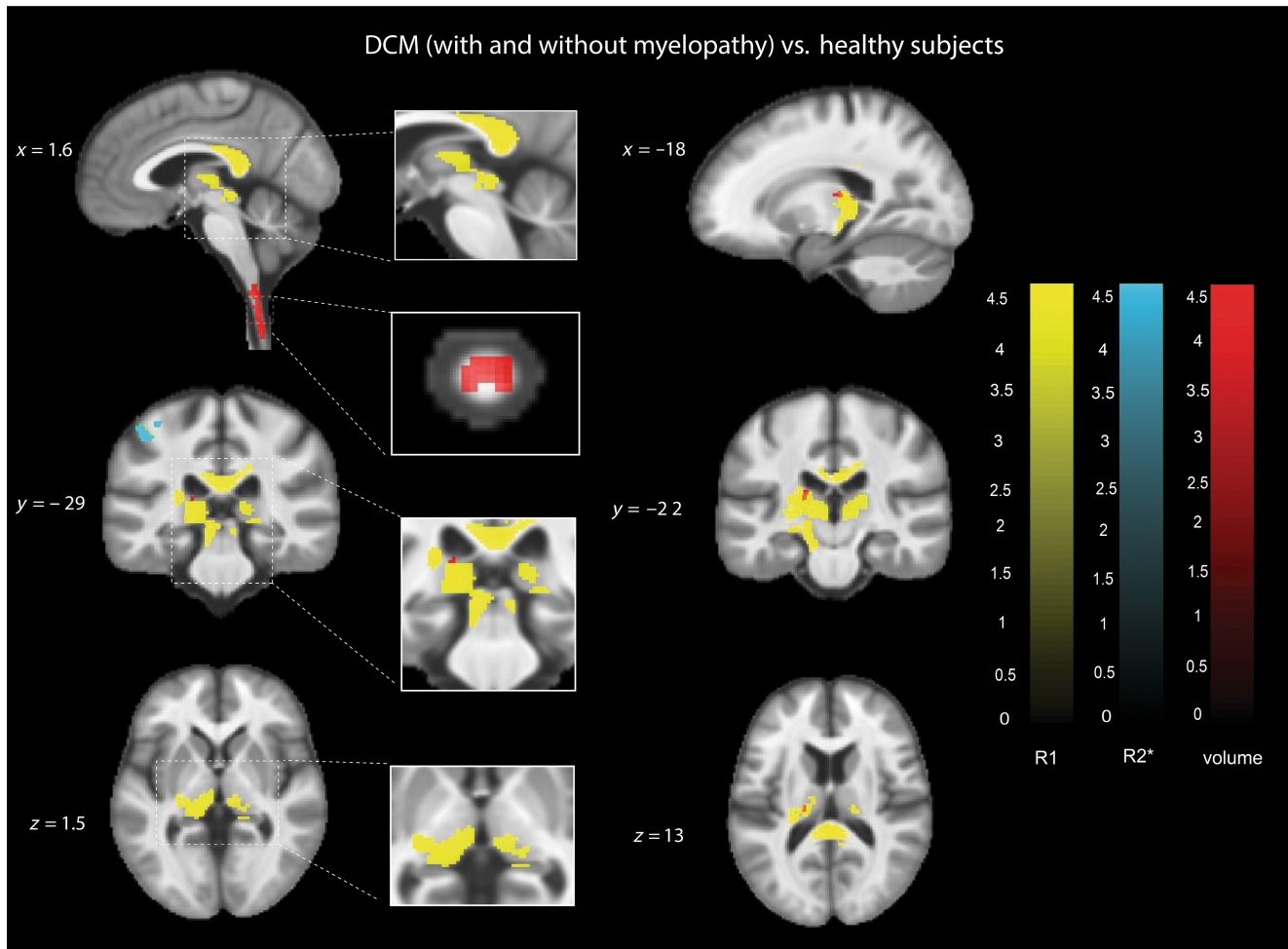
FIGURE 3 Volumetric and microstructural changes (longitudinal relaxation rate [R1] and effective transverse relaxation rate [R2*]) revealed in the degenerative cervical myelopathy (DCM) patients (both with and without myelopathy) when compared to healthy controls. Decreased R1 (yellow) was observed in the thalamus, brainstem periaqueductal grey matter, corpus callosum, and corticospinal tract and increased R2* (blue) in primary somatosensory cortex region in DCM patients compared with healthy controls. Atrophy was also observed in the cervical cord and left thalamus (red). For illustration purposes, the overlay of statistical parametric maps is uncorrected $p < 0.001$ and different slices were chosen, represented with x, y, and z coordinates in Montreal Neurological Institute space. The colour bar indicates the t-score.

TABLE 2 Comparing multiparametric mapping matrices calculated in total degenerative cervical myelopathy group and healthy controls applying the voxel-based quantification and morphometry method.

Parameters	Anatomical area	z-score	p	x, mm	y, mm	z, mm
Atrophy (VBM)	Cervical cord	4.59	0.002	2	−50	−72
	Left thalamus	4.07	0.026	−18	−23	12
R1	Thalamus	4.19	0.001	−15	−33	8
	Midbrain (PAG)	3.91	0.014	−11	−24	−17
	Corpus callosum	4.48	0.0001	3	−39	20
	Corticospinal tract	4.06	0.03	−21	−29	14
R2*	Left S1	4.37	0.008	−44	−32	51

Abbreviations: PAG, periaqueductal grey matter; R1, longitudinal relaxation rate; R2*, transverse relaxation rate; VBM, voxel-based morphometry.

of radiological evidence of myelopathy in this cohort. This may be explained by the compression of spinal arteries, restricting blood supply in the GM and causing ischaemia [37]. Of note, the occurrence of myelopathy was shown to be associated with progressive neuropathological processes such as gliosis and necrosis in the GM of the spinal cord [38].

Assessment of the cervical cord and brain simultaneously

Assessing the entire DCM group simultaneously applying both the brain and spinal cord mapping (SPM-BSC) revealed atrophy and microstructural changes mainly in the sensory regions of the brain.

Performing subgroup analysis showed that these changes are more pronounced in those patients with radiological evidence of myelopathy at the compressed site. Our observation of cervical cord atrophy above the level of compression in DCM patients is in line with previous reports disclosing widespread cord pathology [3, 8]. Atrophy appears to affect the central GM as well as parts of the lateral WM fibre tracts in this cohort, which may be mainly due to vascular impairment induced by stenosis in DCM [39]. A recent study investigating remote microvascular damage in DCM has shown a robust correlation between blood perfusion impairments and atrophy beyond the lesion site [40]. This finding suggests that alterations in haemodynamics could potentially play a role in the neurodegenerative processes observed in DCM, aligning with the findings of our own investigation in the current study.

Focal damage to the spinal cord also remotely perturbs tissue integrity of ascending and descending tracts [4, 41]. Our observations of neurodegenerative changes (decreased R1 as an indirect measure of myelin changes) in the PAG of DCM patients support the hypothesis of ongoing demyelination within the brainstem [6] extending the loss of tissue integrity from the cervical cord towards the brain. Reduced fibre density within tracts passing through the brainstem to sensorimotor areas has been identified in DCM patients [42]. However, atrophy of the sensorimotor cortices was not observed in our cohort. One possible explanation may be that most patients were only mildly affected, and therefore volumetric changes were not as pronounced yet but may already have been initiated. We identified that within the atrophied thalamus, microstructural alterations sensitive to myelin were occurring in this mild–moderately affected DCM cohort. Decreased R1, increased R2*, and concomitant atrophy provide evidence for ongoing neurodegenerative changes indirectly, driven by the presence of myelopathy of the cervical cord. These findings are in line with studies conducted in traumatic spinal cord injury patients [43, 44]. In spinal cord injury, decreased GM volume in the right thalamus was paralleled by increased iron-sensitive R2* values 2 years after acute traumatic spinal cord injury [44]. It has been suggested that the observed iron accumulation was caused by oxidative stress and chronic inflammation provoking myelin breakdown. Several studies [5, 45] have already investigated the role of the thalamus in the progression of DCM. However, most studies focused on macrostructural changes such as volumetric measures or modified connectivity [5]. Previous studies showed that chronic cervical cord compression results in compromised tissue integrity of spinal GM and WM tracts, which ultimately affect the thalamus [5, 45]. Our findings together with previous reports emphasize the involvement of thalamic sensory nuclei in ongoing degeneration in DCM patients. Interestingly, microstructural changes revealed in the posterior part of the corpus callosum support the hypothesis that progressive compression impacts distantly lying regions of the neuroaxis. Postmortem human and primate studies discovered a topographical organization within the corpus callosum, disclosing that some of the posterior fibres connect the parietal cerebral hemispheres and integrate somatosensory information [46]. Previously abnormal diffusion patterns in the corpus callosum of DCM patients were demonstrated indicating ongoing demyelination and inflammation [45]. Therefore, reduced directional coherence of axonal projections of WM tracts including the corpus callosum are believed to be a consequence of chronic spinal cord compression [45], which is in line with the correlation of remote neurodegeneration with clinical impairment.

Sensory and prehension impairments were found to be associated with increased R2* values in the thalamus of all DCM patients. Importantly, there was also a correlation between sensory and prehension impairments and elevated R2* values in the brainstem. Our

TABLE 3 Comparing multiparametric mapping matrices calculated in subgroups of DCM (i.e., groups with and without radiological evidence of myelopathy) and HCs applying the voxel-based quantification and morphometry method.

| Parameters	Anatomical area	Contrast	z-score	p	x, mm	y, mm	z, mm
Atrophy (VBM)	Cervical cord	DCM with myelopathy < HCs	3.39	0.027	2	−48	−72
	Left thalamus	DCM with myelopathy < HCs	4.07	0.023	−18	−22	10
R1	Left thalamus	DCM with myelopathy < HCs	3.48	0.015	−20	−27	8
	Right thalamus	DCM with myelopathy < HCs	3.41	0.029	15	−34	8
	Midbrain (PAG)	DCM with myelopathy < HCs	3.11	0.049	−10	−24	−16
	Corpus callosum	DCM with myelopathy < HCs	3.92	0.0001	3	−40	21
R2*	Corticospinal tract	DCM with myelopathy > HCs	4.42	0.005	22	−12	−8
	Cervical cord	DCM without myelopathy > HCs	3.59	0.024	−2	−50	−98

Abbreviations: HC, healthy control; VBM, voxel-based morphometry; DCM, degenerative cervical myelopathy; R1, longitudinal relaxation rate; R2*, effective transverse relaxation rate; PAG, periaqueductal grey matter.

FIGURE 4 Visualization of correlation between Graded Redefined Assessment of Strength, Sensibility and Prehension (GRASSP) sensation scores of the GRASSP test and effective transverse relaxation rate (R2*) changes in DCM patients with and without myelopathy (n = 33) revealed by voxel-based morphometry. Overlay of statistical parametric maps shows a significant R2* increased in midbrain (mainly periaqueductal grey matter) and thalamus. Different slices were chosen, represented with x, y, and z coordinated in Montreal Neurological Institute space. The colour bar indicates the t-score.
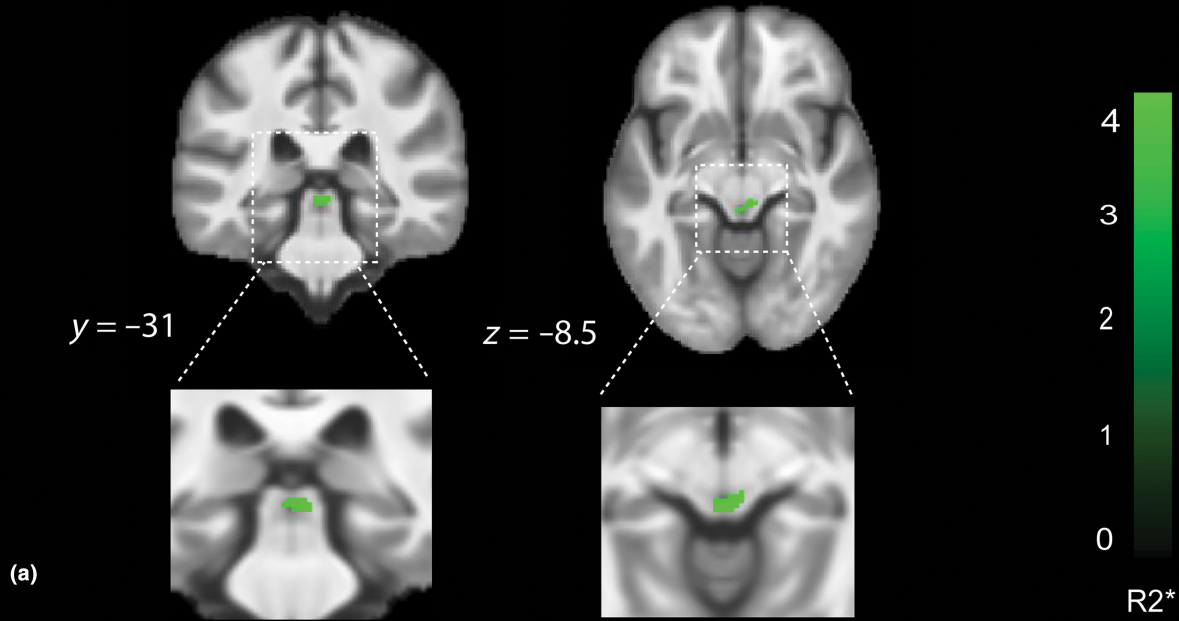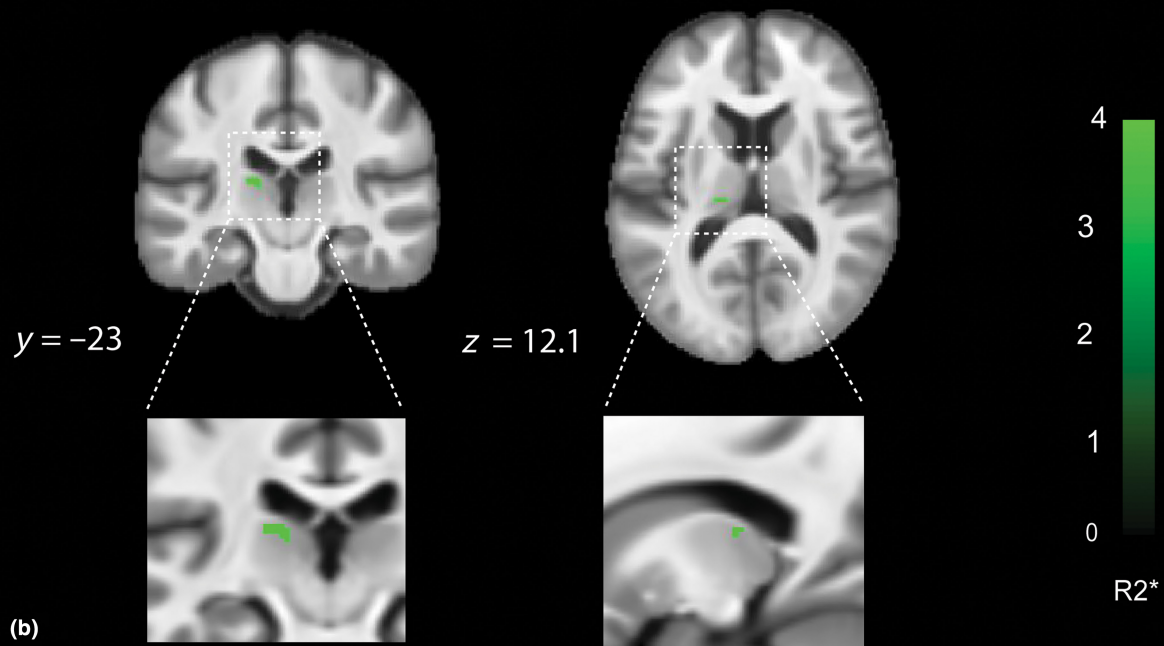
research highlights the significance of thalamus and brainstem integration and suggests that microstructural changes in these supraspinal regions contribute to the severity of observable impairments.

LIMITATIONS

It is necessary to address several limitations of this study. DCM patients were on average 17 years older than the healthy controls. Hence, we adjusted any linear effect of age by adding it as a covariant of no interest in all statistical analyses. Moreover, statistical parametric maps generated by the SPM model are only indirect markers for microstructural changes in biological tissue. Histological samples have shown links between myelination and the parameters of R1 and MT, as well as between R2* and iron content. Therefore, they can be used to investigate underlying tissue properties. Conducting a single scan covering both the brain and spinal cord may provide suboptimal results in terms of different resolution needs in the spinal cord. Although our approach aimed to investigate simultaneous changes between brain and spinal cord and balance time constraints, we acknowledge the potential implications of this trade-off. Although the multicentre nature of the study is crucial for advancing towards identifying biomarkers for clinical trials, it is worth noting that the identical Siemens MRI scanner model was employed across both sites. This study was planned as a cross-sectional design, disclosing information about only one time point. Longitudinal collection of data could enable the investigation of microstructural changes in relation to a temporal dimension and thus allow improved monitoring of disease progression.

In conclusion, this study successfully implemented a simultaneous mapping of spinal cord and brain based on a qMRI protocol within a multicentre study. We found that in mild–moderate DCM, simultaneous qMRI assessments revealed (micro-)structural changes above the compression site in the brain and cervical cord of DCM patients with radiological evidence of myelopathy (T2-weighted hyperintensity at the compression site). These findings disclose the consistent involvement of regions along the whole somatosensory processing stream in mild to moderate DCM. Neurodegeneration in supraspinal regions was associated with greater prehension impairment, indicating that these regions are the dominantly disturbed pathways affected by DCM.

AUTHOR CONTRIBUTIONS

Maryam Seif: Conceptualization; investigation; validation; methodology; formal analysis; data curation; supervision; writing – original draft; writing – review and editing; funding acquisition; visualization. **Patrick Freund:** Conceptualization; writing – review and editing; resources; funding acquisition. **Viveka Boller:** Methodology; software; formal analysis; writing – original draft. **Tim M. Emmenegger:** Methodology; formal analysis; writing – review and editing. **Muhammad Akbar:** Data curation. **Markus Hupp:** Data curation. **Nikolai Pfender:** Data curation. **Claudia Angela Michela Gandini Wheeler-Kingshott:** Funding acquisition; writing – review and editing. **Julien Cohen-Adad:** Writing – review and editing. **Michael G. Fehlings:** Conceptualization. **Armin Curt:** Conceptualization; resources.

CONFLICT OF INTEREST STATEMENT

The authors declare that the research was conducted in the absence of any commercial or financial relationships that could be construed as a potential conflict of interest.

DATA AVAILABILITY STATEMENT

The data that support the findings of this study are available on request from the corresponding author. The data are not publicly available due to privacy or ethical restrictions.

ETHICS STATEMENT

This prospective study was in accordance with the Declaration of Helsinki, approved by the local Ethics Committee (EK-2010-0271, 16-5149-AE), and registered (www.clinicaltrials.gov; NCT 02170155) in Zurich and Toronto. Informed written consent was obtained from each participant before study enrolment.

STUDY SUBJECTS OR COHORTS OVERLAP

Of note, a subset of the data presented in this study (the participants who were recruited in Zurich) have been reported in previous studies [4, 41] assessing remote neurodegeneration in the lumbar cord.

ORCID

Tim M. Emmenegger https://orcid.org/0000-0003-0350-3482
Maryam Seif https://orcid.org/0000-0002-9253-5680

REFERENCES

1. Kalsi-Ryan S, Riehm LE, Tetreault L, et al. Characteristics of upper limb impairment related to degenerative cervical myelopathy: development of a sensitive hand assessment (graded redefined assessment of strength, sensibility, and prehension version myelopathy). *Clin Neurosurg.* 2020;86:E292-E299.
2. Badhiwala JH, Ahuja CS, Akbar MA, et al. Degenerative cervical myelopathy—update and future directions. *Nat Rev Neurol.* 2020;16:108-124.

3. Seif M, David G, Huber E, Vallotton K, Curt A, Freund P. Cervical cord neurodegeneration in traumatic and non-traumatic spinal cord injury. *J Neurotrauma.* 2019;37:860-867.

4. Vallotton K, David G, Hupp M, et al. Tracking white and gray matter degeneration along the spinal cord Axis in degenerative cervical myelopathy. *J Neurotrauma.* 2021;38:2978-2987.

5. Bernabéu-Sanz Á, Mollá-Torró JV, López-Celada S, Moreno López P, Fernández-Jover E. MRI evidence of brain atrophy, white matter damage, and functional adaptive changes in patients with cervical spondylosis and prolonged spinal cord compression. *Eur Radiol.* 2020;30:357-369.

6. Filimonova E, Vasilenko I, Kubetsky Y, Prokhorov O, Abdaev M, Rzaev J. Brainstem and subcortical regions volume loss in patients with degenerative cervical myelopathy and its association with spinal cord compression severity. *Clin Neurol Neurosurg.* 2023;233:107943.

7. Grabher P, Mohammadi S, Trachsler A, et al. Voxel-based analysis of grey and white matter degeneration in cervical spondylotic myelopathy. *Sci Rep.* 2016;6:24636.

8. Grabher P, Mohammadi S, David G, Freund P. Neurodegeneration in the spinal ventral horn prior to motor impairment in cervical Spondylotic myelopathy. *J Neurotrauma.* 2017;34:2329-2334.

9. Martin A, De Leener B, Cohen-Adad J, et al. Monitoring for myelopathic progression with multiparametric quantitative MRI. In: Toft M, ed. *2017 CSRS Annual Meeting.* Public Library of Science; 2017:e0195733.

10. Chen X, Kong C, Feng S, et al. Magnetic resonance diffusion tensor imaging of cervical spinal cord and lumbosacral enlargement in patients with cervical spondylotic myelopathy. *J Magn Reson Imaging.* 2016;43:1484-1491.

11. Cui L, Kong C, Chen X, Liu Y, Zhang Y, Guan Y. Changes in diffusion tensor imaging indices of the lumbosacral enlargement correlate with cervical spinal cord changes and clinical assessment in patients with cervical spondylotic myelopathy. *Clin Neurol Neurosurg.* 2019;186:105282.

12. Martin AR, Aleksanderek I, Cohen-Adad J, et al. Translating state-of-the-art spinal cord MRI techniques to clinical use: a systematic review of clinical studies utilizing DTI, MT, MWF, MRS, and fMRI. *NeuroImage Clin.* 2016;10:192-238.

13. Leutritz T, Seif M, Helms G, et al. Multiparameter mapping of relaxation (R1, R2*), proton density and magnetization transfer saturation at 3 T: a multicenter dual-vendor reproducibility and repeatability study. *Hum Brain Mapp.* 2020;41:4232-4247.

14. Cohen-Adad J, Alonso-Ortiz E, Abramovic M, et al. Open-access quantitative MRI data of the spinal cord and reproducibility across participants, sites and manufacturers. *Sci Data.* 2021;81(8):1-17.

15. Lukas C, Bellenberg B, Prados F, et al. Quantification of cervical cord cross-sectional area: which acquisition, vertebra level, and analysis software? A multicenter repeatability study on a traveling healthy volunteer. *Front Neurol.* 2021;12:1153.

16. Seif M, Leutritz T, Schading S, et al. Reliability of multi-parameter mapping (MPM) in the cervical cord: a multi-center multi-vendor quantitative MRI study. *NeuroImage.* 2022;264:119751.

17. Blaiotta C, Freund P, Cardoso MJ, Ashburner J. Generative diffeomorphic modelling of large MRI data sets for probabilistic template construction. *NeuroImage.* 2018;166:117-134.

18. Azzarito M, Kyathanahally SP, Balbastre Y, et al. Simultaneous voxel-wise analysis of brain and spinal cord morphometry and microstructure within the SPM framework. *Hum Brain Mapp.* 2021;42:220-232.

19. Freund P, Papinutto N, Bischof A, et al. Simultaneous assessment of regional distributions of atrophy across the neuraxis in MS patients. *NeuroImage Clin.* 2022;34:102985.

20. Fehlings MG, Badhiwala JH, Ahn H, et al. Safety and efficacy of riluzole in patients undergoing decompressive surgery for degenerative cervical myelopathy (CSM-protect): a multicentre, double-blind, placebo-controlled, randomised, phase 3 trial. *Lancet Neurol.* 2021;20:98-106.

21. Tetreault L, Kopjar B, Nouri A, et al. The modified Japanese Orthopaedic association scale: establishing criteria for mild, moderate and severe impairment in patients with degenerative cervical myelopathy. *Eur Spine J.* 2017;26:78-84.

22. Nurjck S. The pathogenesis of the spinal cord disorder associated with cervical spondylosis. *Brain.* 1972;95:87-100.

23. Kalsi-Ryan S, Curt A, Verrier MC, Fehlings MG. Development of the graded redefined assessment of strength, sensibility and prehension (GRASSP): reviewing measurement specific to the upper limb in tetraplegia. *J Neurosurg Spine.* 2012;17:65-76.

24. Kirshblum SC, Burns SP, Biering-Sorensen F, et al. International standards for neurological classification of spinal cord injury (revised 2011). *J Spinal Cord Med.* 2011;34:535-546.

25. Weiskopf N, Suckling J, Williams G, et al. Quantitative multi-parameter mapping of R1, PD*, MT, and R2* at 3T: a multi-center validation. *Front Neurosci.* 2013;7:95.

26. Helms G, Dathe H, Dechent P. Quantitative FLASH MRI at 3T using a rational approximation of the Ernst equation. *Magn Reson Med.* 2008;59:667-672.

27. De Leener B, Fonov VS, Collins DL, Callot V, Stikov N, Cohen-Adad J. PAM50: unbiased multimodal template of the brainstem and spinal cord aligned with the ICBM152 space. *NeuroImage.* 2018;165:170-179.

28. De Leener B, Lévy S, Dupont SM, et al. SCT: spinal cord toolbox, an open-source software for processing spinal cord MRI data. *NeuroImage.* 2017;145:24-43.

29. Ashburner J. A fast diffeomorphic image registration algorithm. *NeuroImage.* 2007;38:95-113.

30. Good CD, Johnsrude IS, Ashburner J, Henson RNA, Friston KJ, Frackowiak RSJ. A voxel-based morphometric study of ageing in 465 normal adult human brains. *NeuroImage.* 2001;14:21-36.

31. Malone IB, Leung KK, Clegg S, et al. Accurate automatic estimation of total intracranial volume: a nuisance variable with less nuisance. *NeuroImage.* 2015;104:366-372.

32. Tabelow K, Balteau E, Ashburner J, et al. hMRI – a toolbox for quantitative MRI in neuroscience and clinical research. *NeuroImage.* 2019;194:191-210.

33. Weiskopf N, Lutti A, Helms G, Novak M, Ashburner J, Hutton C. Unified segmentation based correction of R1 brain maps for RF transmit field inhomogeneities (UNICORT). *NeuroImage.* 2011;54:2116-2124.

34. Ashburner J, Friston KJ. Unified segmentation. *NeuroImage.* 2005;26:839-851.

35. Freund P, Weiskopf N, Ashburner J, et al. MRI investigation of the sensorimotor cortex and the corticospinal tract after acute spinal cord injury: a prospective longitudinal study. *Lancet Neurol.* 2013;12:873-881.

36. Grabher P, Callaghan MF, Ashburner J, et al. Tracking sensory system atrophy and outcome prediction in spinal cord injury. *Ann Neurol.* 2015;78:751-761.

37. Ellingson BM, Woodworth DC, Leu K, Salamon N, Holly LT. Spinal cord perfusion MR imaging implicates both ischemia and hypoxia in the Pathogenesis of cervical spondylosis. *World Neurosurg.* 2019;128:e773-e781.

38. Gibson J, Nouri A, Krueger B, et al. Degenerative cervical myelopathy: a clinical review. *Yale J Biol Med.* 2018;91:43-48.

39. Karadimas SK, Gatzounis G, Fehlings MG. Pathobiology of cervical spondylotic myelopathy. *Eur Spine J.* 2015;24:132-138.

40. Lebret A, Lévy S, Pfender N, et al. Investigation of perfusion impairment in degenerative cervical myelopathy beyond the site of cord compression. *Sci Rep.* 2023;13:22660.

41. David G, Vallotton K, Hupp M, Curt A, Freund P, Seif M. Extent of cord pathology in the lumbosacral enlargement in non-traumatic versus traumatic spinal cord injury. *J Neurotrauma.* 2022;39:639-650.

42. Wang X, Zhou T, Maynard GD, et al. Nogo receptor decoy promotes recovery and corticospinal growth in non-human primate spinal cord injury. *Brain*. 2020;143:1697-1713.

43. Freund P, Curt A, Hupp M, et al. *Progressive atrophy, prediction and potential endpoints for trials in acute spinal cord injury*. OHBM Honolulu; 2015.

44. Ziegler G, Grabher P, Thompson A, et al. Progressive neurodegeneration following spinal cord injury. *Neurology*. 2018;90:e1257-e1266.

45. Wang C, Laiwalla A, Salamon N, Ellingson BM, Holly LT. Compensatory brainstem functional and structural connectivity in patients with degenerative cervical myelopathy by probabilistic tractography and functional MRI. *Brain Res*. 2020;1749:147129.

46. Fabri M, Polonara G, Mascioli G, Salvolini U, Manzoni T. Topographical organization of human corpus callosum: an fMRI mapping study. *Brain Res*. 2011;1370:99-111.